


Mechanistic Insights into Water Autoionization through Metadynamics Simulation Enhanced by Machine Learning

Ling Liu^{✉,*}, Yingqi Tian[✉], Xuanye Yang[✉], and Chungeng Liu^{✉,†}

Institute of Theoretical and Computational Chemistry, School of Chemistry and Chemical Engineering, Nanjing University, Nanjing 210023, China

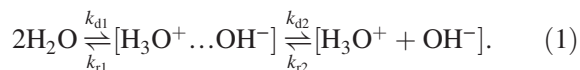
 (Received 2 August 2022; revised 5 July 2023; accepted 21 August 2023; published 9 October 2023)

Characterizing the free energy landscape of water ionization has been a great challenge due to the limitations from expensive *ab initio* calculations and strong rare-event features. Lacking equilibrium sampling of the ionization pathway will cause ambiguities in the mechanistic study. Here, we obtain convergent free energy surfaces through nanosecond timescale metadynamics simulations with classical nuclei enhanced by atomic neural network potentials, which yields good reproduction of the equilibrium constant ($pK_w = 14.14$) and ionization rate constant ($1.369 \times 10^{-3} \text{ s}^{-1}$). The character of transition state unveils the triple-proton transfer occurs through a concerted but asynchronous mechanism. Conditional ensemble average analyses establish the dual-presolvation mechanism, where a pair of hypercoordinated and undercoordinated waters bridged by one H_2O cooperatively constitutes the initiation environment for autoionization, and contributes extremely to the local electric field fluctuation to promote water dissociation.

DOI: 10.1103/PhysRevLett.131.158001

Water serves as the most basic and common substance involved in a wide variety of chemical processes and living organisms [1–3]. The autoionization of a liquid water molecule to a pair of H^+ and OH^- plays a critical role in determining pH and conductivity. Being a long-standing interest for experiment and theory, however, the exploration of the mechanism is obstructed by the striking stability difference between water and dissociated ions [4,5], which gives rise to the severe multiscale kinetics feature of the ionization process, and impractical macroscopic-timescale propagation of the hydrogen-bond network dynamics.

Decades ago, Eigen and De Mayer proposed that the initial dissociation of a water system is the dynamical bottleneck for autoionization, where the formed H_3O^+ and OH^- ions reach the so-called contact distance, followed by a relatively facile diffusion away from each other [4]. The entire process can be expressed using the following model:



It was later employed by Natzle *et al.* in an experimental study of the transient conductivity in photoionized water system [5]. Based on Eigen's assumption that the reverse recombination rate is controlled by diffusion of free ions ($k_{r1} \gg k_{r2}$), the contact distance in $[\text{H}_3\text{O}^+ \dots \text{OH}^-]$ was characterized as $5.8 \pm 0.5 \text{ \AA}$, corresponding to an ion-pair separation by two waters. Meanwhile, the overall recombination rate constant, approximately equal to k_{r2} , was determined as $0.112 \text{ M}^{-1} \text{ ps}^{-1}$, and the dissociation rate constant was estimated as $2.04 \times 10^{-5} \text{ s}^{-1}$ by taking the well-characterized

ionization equilibrium constant. Because of the extremely scarce probability of water dissociation in natural conditions, directly tracking the autoionization process of a specific water molecule still remains a tough task today.

Theoretical study has demonstrated its irreplaceable role to complement experimental exploration of the mechanism [6–10]. By inspecting the neutralization features from *ab initio* molecular dynamics (AIMD) trajectories, Hassanali *et al.* deduced that water ionization goes through a concerted triple-proton jump, which is triggered by a collective compression of the reactive four-water wire and the presolvation phenomenon characterized as the hypercoordination of the dissociating water [9]. However, a lack of guarantee for equilibrium sampling of structural distributions in standard AIMD may bring uncertainty to the simulation results. Introducing the path-sampling methods into AIMD is an effective solution to rare-event sampling [11]. On this basis, Geissler *et al.* suggested that water dissociation can be substantially accelerated by the solvent-induced electric field [8,12], while the physical picture behind the electric field fluctuations has not been explicitly revealed. More recently, Moqadam *et al.* proposed that the dissociation event is likely to occur through a double-proton jump, leaving the third proton transfer in a stepwise way [10]. Thus, the ambiguity in ionization mechanism needs to be clarified.

Quantifying the free energy landscape is of paramount importance in understanding the water ionization mechanism. Herein, we employ the well-tempered metadynamics to characterize the ionization free energy profiles [13,14]. A series of collective variables (CVs) is specifically designed

to monitor the proton transfer progress and the evolution of concerned properties. Considering the deep potential well in neutral water state, a nanosecond (ns) timescale is required to ensure the convergence of free energy profiles and hence the sufficient statistical sampling of ionization path, which is inaccessible to the conventional *ab initio* calculation. To overcome the computational bottleneck, atomic neural network potentials (NNPs) are employed to replace the time-consuming density functional theory (DFT) calculation [15,16]. We will show that the equilibrium constant and rate constant of water autoionization deduced from the classical free energy surface are in quantitative agreement with the documented experimental results. The nuclear quantum effects (NQEs) investigated by combing path integral approach [3,17] are found to have a pronounced effect on the equilibrium probability distribution. By looking into the structural evolution along the CVs, we will unveil the asynchronous nature of concerted triple-proton transfer along the hydrogen-bonded water wire, and propose the dual-presolvation mechanism which contributes to the electric field fluctuations on triggering water ionization.

In performing metadynamics simulations, bias is applied to two CVs that relate to the number of ions and the distance between ionic species (Equation S5 and S6 in the Supplemental Material [18]), allowing the water dissociation to take place anywhere in a 64-water box. Up to 10 ns of simulation time is proved to guarantee the convergence of free energy differences and hence the proper statistical sampling along the concerned reaction pathway (Fig. S3 [18]). Finite size effects are checked to be minimal by extending the simulation to the 512-water system (Fig. S5 [18]). All the technical details of simulations can be found in the Supplemental Material [18].

Considering the existence of $[\text{H}_3\text{O}^+ \dots \text{OH}^-]$ pair at the contact distance, we base on a dynamically assigned four-water wire to design new CVs for constructing free energy surface, as illustrated in Fig. 1. $\sum_3 \delta(\text{O}-\text{H})$ and $\sum_3 R(\text{O}-\text{O})$ represent the coordinates of triple-proton transfer and total water wire length, respectively. The proton transfer is supposed to proceed in two possible routes, along the H_3O^+ and OH^- directions. The routes differ in the nature of the species the proton (e.g., H_c in Fig. 1) transfers to and from during the dissociation process.

The ionization free energy profiles are computed by reweighting the biased probability density [19] as a function of the defined CVs. We use the nudged elastic band (NEB) method [54] to determine the minimum free energy path and transition state (TS) on this two-dimensional (2D) CV space. As seen in Fig. 2(a), the overall transfer progress of the involved three protons is strongly coupled with the compression of the whole water wire, showing good consistency with the previous AIMD study [9]. The unique TS located in the free energy surface indicates a concerted triple-proton transfer within an elementary reaction step. The corresponding

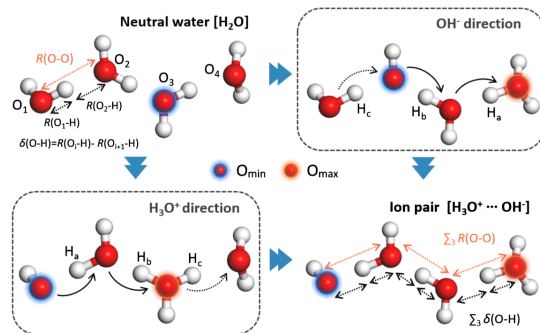


FIG. 1. Schematic diagram of the evolution of four-water wires during water dissociation, where the proton transfer proceeds in two possible ways, along the H_3O^+ and OH^- directions. The hydrogen-bonded wire is determined through searching for the shortest connection between the most negatively and positively charged O centers, O_{\min} and O_{\max} , in each metadynamics configuration (see Fig. S7 [18] for details). The three bridging hydrogen atoms are labeled H_a , H_b , and H_c , according to the sequence of proton transfer progress (by comparing the elongated O—H lengths), and O— H_a is required to be the longest.

free energy barrier can be easily determined by extracting the free energies of critical points along the NEB path [Fig. 2(b)]. In the classical case, the forward (dissociation) and backward (recombination) activation free energies, ΔG_D^\ddagger and ΔG_R^\ddagger , are calculated to be 78.991 ± 0.657 and 1.665 ± 0.218 kJ/mol, respectively, as an average of three independent metadynamics simulations (Fig. S3 [18]). A correction of +0.349 kJ/mol has been added to the free energies of both TS and the ion-pair state for setting 1 M concentration as the reference.

By applying variational transition state theory [55,56], the calculated elementary rate constants for water dissociation (k_{d1}) to form the ion-pair intermediate and the backward neutralization (k_{r1}) are listed in Table I. The calculated k_{d1} is on the same scale with 0.011 s^{-1} evaluated from the path sampling simulation [10]. The ion pair at the contact distance recombines with a frequency of

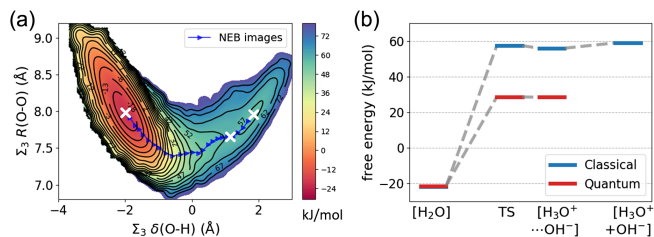


FIG. 2. (a) Free energy surface (with classical nuclei) constructed with $\sum_3 \delta(\text{O}-\text{H})$ and $\sum_3 R(\text{O}-\text{O})$. The connected blue triangles denote the optimized NEB images. (b) Free energy diagrams of the critical points obtained from classical and path integral metadynamics, including neutral water $[\text{H}_2\text{O}]$, TS and ion-pair intermediate $[\text{H}_3\text{O}^+ \dots \text{OH}^-]$, marked with “ \times ” in (a). The well-separated ionic state $[\text{H}_3\text{O}^+ + \text{OH}^-]$ is evaluated by adding ΔE_{cl} .

TABLE I. Comparison of theoretical and experimental kinetic parameters for water ionization at 298 K.

	This Letter	Experiment [5]
k_{d1} (s^{-1})	0.077 ± 0.020	...
k_{d2} (ps^{-1})	0.0574^a	0.0661
k_{r1} (ps^{-1})	3.171 ± 0.278	...
k_{r2} (ps^{-1})	0.101^a	0.112
k_D (s^{-1})	1.369×10^{-3}	1.132×10^{-3b}
k_R (ps^{-1})	0.189^c	0.112
K_w^d	$(0.724 \pm 0.202) \times 10^{-14}$	1×10^{-14}

^aCalculated by the equations in Ref. [5] (details in Supplemental Material [18]).

^bThe original $2.04 \times 10^{-5} s^{-1}$ deduced from $K_w k_R / c_{H_2O}$ has been multiplied with c_{H_2O} of 55.5 M.

^cCalculated by k_D / K_w .

^d K_w is dimensionless since the concentration unit in all rate constants is removed by utilizing the standard concentration c^\ominus .

approximately $2.75 ps^{-1}$ when taking into account the ionic concentration ($\sim 0.869 M$) in the simulated box, which agrees well with the timescale of $\sim 0.5 ps$ for recombination events [9]. The equilibrium constant K_w of water autoionization can be feasibly obtained, after introducing the electrostatic energy correction (ΔE_{el}) for the further ion-pair separation from contact distance R_{cd} to infinity (forming $[H_3O^+ + OH^-]$). ΔE_{el} is estimated as the negative of Coulomb attractive energy between two unit point charges separated by R_{cd} , which is determined as 5.928 \AA from the ensemble average algorithm [Eq. (S9)]. K_w is then calculated with $k_{d1}/k_{r1} \exp(-\Delta E_{el}/RT)$ as 0.724×10^{-14} . The value ($pK_w = 14.14$) is quite close to the well-known experimental result, and shows a higher accuracy than the calculation results from constrained AIMD [6,7] and a recent umbrella sampling simulation [57]. The identification of local minimum and TS is fairly ambiguous in those studies which mainly ascribes to the inappropriately chosen reaction coordinates.

By inspecting Table I, we can conclude that the water dissociation step is rate determining in the overall autoionization process, as the rate constant k_{d1} is 12 orders of magnitude lower than that of the diffusion step of ion pair (k_{d2}). Accordingly, it is reasonable to make the steady-state approximation in the calculation of overall ionization rate constant k_D . Being formulated with $k_{d1}k_{d2}/(k_{d2} + k_{r1})$, k_D is determined as $1.369 \times 10^{-3} s^{-1}$. Obviously, the calculated k_D and k_R are in quantitative agreement with the experimental results.

Since the nuclei are quantum particles in nature, NQEs have to be taken into account when studying the water ionization process [3,17]. Here we carry out path integral metadynamics simulations [20] with atomic forces calculated from NNPs to build the quantum free energy landscape (see Supplemental Material [18] for technical details). As compared in Fig. 2(b), the relative stability

of ion-pair state is considerably enhanced, corresponding to a decrease of reaction free energy of $\sim 27.8 kJ/mol$. Thus the NQEs will increase the equilibrium constant as well as dissociation rate constant by about 5 orders of magnitude, albeit with severe deviation from the experimental results. This mismatch between quantum free energies and experiment can be explained by a fortuitous cancellation between the NQEs and the electronic interaction ignored in pure density functionals [21]. It miraculously results in the remarkable ability of pure functional (in the form of fitted NNPs) with classical nuclei to reproduce the equilibrium distribution along the ionization pathway, which is of crucial importance for subsequent mechanism analysis. However, exactly decomposing the nuclear and electronic quantum effects remains to be an open question.

To assess the synchronicity of triple-proton jump during water dissociation, we decompose the CV $\sum_3 \delta(O-H)$ into $\delta(O-H_c)$ and $\delta(O-H_a) + \delta(O-H_b)$. A new contour map of classical free energy surface, shown in Fig. 3(a), is then constructed by the two decomposed CVs, with $\sum_3 R(O-O)$ integrated out in recounting the distribution of biased probability density. The TS is characterized with a quite positive value of $\sum_2 \delta(O-H)$ and a nearly zero value of $\delta(O-H_c)$, indicating the transfers of H_a and H_b have been almost finished, while the transfer of H_c is on the half way [Fig. 3(b)]. Following the definitions of concerted and synchronous reactions [58–60], we establish that water autoionization takes place through a concerted and asynchronous proton transfer (PT) mechanism. This explains why there was a longer waiting time between the second and third PT event in the path sampling simulation [10].

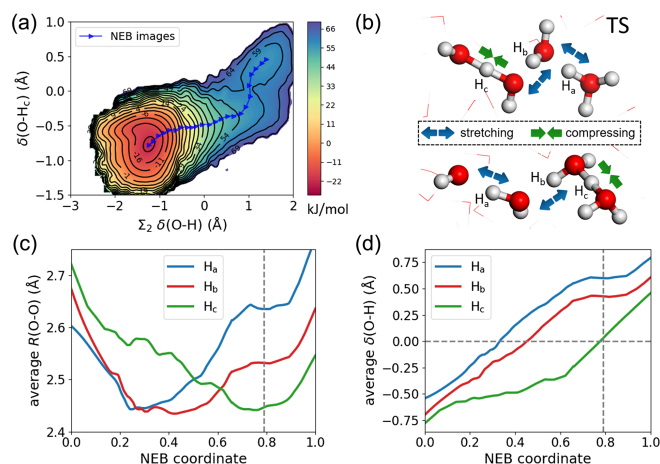


FIG. 3. (a) Free energy surface (with classical nuclei) constructed with $\delta(O-H_c)$ and $\delta(O-H_a) + \delta(O-H_b)$. (b) Illustrative snapshots of TS for the OH^- (top) and H_3O^+ (bottom) directions. The arrow denotes the direction of oxygen motions before reaching TS. Evolution of conditional ensemble average of (c) $R(O-O)$ and (d) $\delta(O-H)$ along the normalized NEB coordinate. The vertical line marks the location of TS.

Tracking the evolution of each pairwise oxygen distance $R(\text{O}-\text{O})$ and $\delta(\text{O}-\text{H})$ along the PT coordinate allows a deeper insight into the cooperative relation between oxygen and proton motions, which can be extracted from the 2D reweighted distributions (Fig. S8 [18]) based on the conditional ensemble average algorithm introduced in Eq. (S8) [18]. As shown in Fig. 3(c), the oxygen atoms neighboring to H_a and H_b reach their maximal contractions well before the TS, whereas those adjacent to H_c keep compressed until the TS point. Comparison with Fig. 3(d) reveals that the progress of each proton transfer is well controlled by the neighboring oxygen contraction, and interestingly, corresponding to a similar shortest oxygen separation at ~ 2.44 Å. Although H_c transfer is significantly postponed, it still proceeds within a compressed water wire which manifests the weak correlation with the preceding two transfers, thus should not be regarded as a stepwise step.

The excess proton was found to preferentially transfer to the neighboring water that possesses the lowest coordination number (CN) in the acid solution [61], which was later referred to as presolvation. The notion of presolvation can be generalized as the change of coordinated hydrogen bonds (HBs) on the species ready to accept or donate protons that will initiate the PT events [1,62,63]. We investigate the presolvation in water dissociation by tracking the number of accepted HBs around the oxygen atoms involved in the two earlier transfers of H_a and H_b , while the presolvation of H_c transfer exhibits obviously the character like a single PT event due to its delayed feature (Fig. S11 [18]). Given the reported difference of HB patterns between the H^+ and OH^- migration systems [1,61,62], the configurations are further classified into the PT events proceeding along H_3O^+ and OH^- directions. As the two PT modes are found to present similar presolvation phenomena, only the PT event along H_3O^+ direction is discussed below (see Fig. S10 [18] for results along OH^- direction).

As displayed in Fig. 4(a), a concerted transfer route of H_a and H_b is constructed to approximate the minimum free energy path by connecting the neutral water state linearly to an artificially defined ion-pair state separated by one water. The 2D reweighted CN distributions for the three relevant O atoms as functions of PT coordinates are computed and shown in Fig. S9 [18], from which the average CN evolution along the proposed linear transfer path is extracted and plotted against $\delta(\text{O}-\text{H}_a)$. By inspecting Figs. 4(b) and 4(c), the average CN of O_1 increases by ~ 0.4 before $\delta(\text{O}-\text{H}_a)$ reaches zero. It manifests the presolvation phenomenon that a hypercoordinated water is formed prior to H_a transfer as proposed in previous studies [9,10]. The sharp increase from 2.12 to 3.15 of the CN of O_1 (at the dashed line) arises from the change in affiliation of H_a , on leaving from O_1 to O_2 . As H_a transfer finishes, the nascent OH^- is coordinated with nearly four

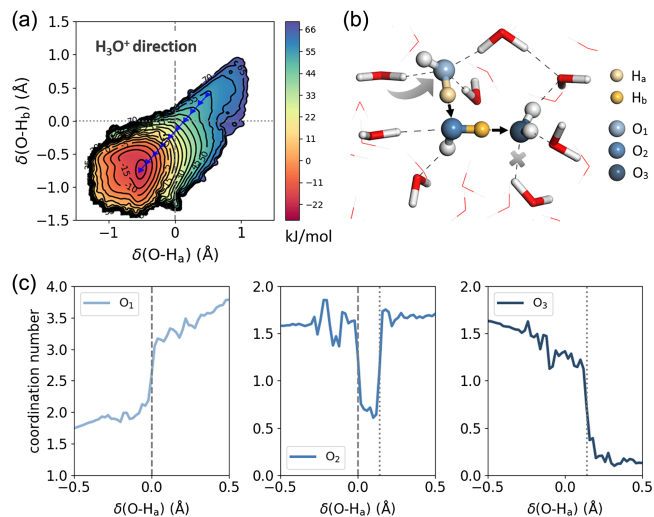


FIG. 4. (a) Free energy surfaces constructed with $\delta(\text{O}-\text{H}_a)$ and $\delta(\text{O}-\text{H}_b)$. A constraint of $\delta(\text{O}-\text{H}_c) < 0$ is applied in the counting to exclude the configurations belonging to the third proton jump stage. (b) An illustrative snapshot of presolvation. (c) Evolution of CN on the three relevant oxygen atoms against $\delta(\text{O}-\text{H}_a)$. The dashed line marks the position where $\delta(\text{O}-\text{H}_a)$ or $\delta(\text{O}-\text{H}_b)$ equals to zero.

accepted HBs, namely the $\text{OH}^-(\text{H}_2\text{O})_4$ complex. However, an opposite trend in the CN evolution of O_3 is observed with a decrease by ~ 0.49 before $\delta(\text{O}-\text{H}_b)$ reaches zero. It unveils the necessity of concurrently forming an under-coordinated water to trigger ionization. After H_b transfer, the nascent H_3O^+ exists as a H_9O_4^+ complex with only three donated HBs coordinated to the ion core. The intermediate O_2 atom exhibits a “relay station” character, because its CN is essentially unchanged except during the short period from $\delta(\text{O}-\text{H}_a) = 0$ to $\delta(\text{O}-\text{H}_b) = 0$. The sudden dropping followed by a quick restoring is due to the change of the affiliated oxygen atoms of H_a and H_b . Accordingly, a dual-presolvation mechanism is proposed for water autoionization [Fig. 4(b)].

Electric field fluctuation was suggested to play a determinative role in water autoionization [8,12]. Here we explore the correlation between the local electric field and the presolvation behavior, as the long-range part contributes minorly to the internal electric field (Figs. S12 and S13) [22]. Taking atomic charges from the SPC/E water model [64], the local electric fields on the migrating H_a and H_b are estimated roughly with Coulomb’s law, while restricting the contribution from waters within the first solvation shell around the water wire. A new CV labeled E_1 is defined as the projection of local electric field on the dissociating $\text{O}-\text{H}$ bond, such that a positive E_1 is expected to push the protons to dissociation.

By projecting the configurations into the 2D histogram plots of E_1 and CN of relevant oxygen atoms, Fig. 5 shows directly the regular patterns of structure distributions in the

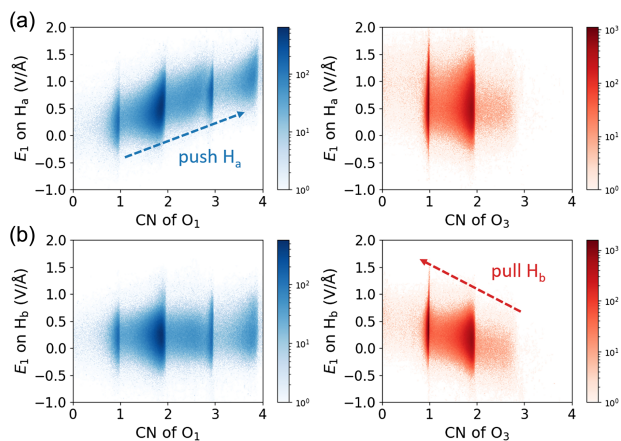


FIG. 5. Histogram plots in a logarithmic scale of metadynamics configurations described by the CN of O_1/O_3 and E_1 on (a) H_a and (b) H_b . The constraint of $\delta(O-H_c) < 0$ is applied as well. Blue and red colors represent the oxygens to be transformed to OH^- and H_3O^+ .

H_3O^+ direction of double-proton transfer. The larger CN of O_1 contributes mainly to the stronger electric field on H_a , a trend also noted in a classical MD study [22], which is, however, much less sensitive to the CN of O_3 . Contrarily, E_1 on H_b shows an increasing trend as the CN of O_3 decreases, but the CN of O_1 makes little effect. The results demonstrate that the accepted HB of the dissociating water will pose a repulsive electrostatic force on the proton H_a to facilitate its leaving (push effect). And the breakage of accepted HB on the proton-receiving water will reduce the repulsion, which in turn attracts the arrival of proton H_b (pull effect). Consequently, both hypercoordinated and undercoordinated waters in the dual-presolvation mechanism are suggested to be correlated with strong electric fields on the nearest migrating protons, and a similar conclusion holds for the OH^- direction of PT (Fig. S13 [18]).

To tackle the rare-event difficulty, this Letter implements the machine learning-assisted metadynamics that enables the equilibrium sampling of water dissociation pathway. Critical intermediate and transition state are clearly characterized in the classical free energy landscape, which also reproduces the equilibrium and rate constants of autoionization. Seeking a comprehensive understanding of the mechanism, we unveil the asynchronous character in the concerted triple-proton transfer, and elucidate the solvent-driven phenomena, including dual-presolvation and local electric field fluctuations, in the ionization process. These new findings will be referable for a great variety of water-participated processes.

We thank Professors Yi Gao and Ye Mei for constructive suggestions. This work is supported by the National Key Research and Development Program of China

(2022YFA1503103) and the National Natural Science Foundation of China (22073041). We thank the High Performance Computing Center of Nanjing University for computational resources.

*Corresponding author: lingliu@nju.edu.cn

†Corresponding author: cgliu@nju.edu.cn

- [1] D. Marx, A. Chandra, and M. E. Tuckerman, Aqueous basic solutions: Hydroxide solvation, structural diffusion, and comparison to the hydrated proton, *Chem. Rev.* **110**, 2174 (2010).
- [2] N. Agmon, H. J. Bakker, R. K. Campen, R. H. Henchman, P. Pohl, S. Roke, M. Thämer, and A. Hassanali, Protons and hydroxide ions in aqueous systems, *Chem. Rev.* **116**, 7642 (2016).
- [3] M. Ceriotti, W. Fang, P. G. Kusalik, R. H. McKenzie, A. Michaelides, M. A. Morales, and T. E. Markland, Nuclear quantum effects in water and aqueous systems: Experiment, theory, and current challenges, *Chem. Rev.* **116**, 7529 (2016).
- [4] M. Eigen, L. De Maeyer, and J. D. Bernal, Self-dissociation and protonic charge transport in water and ice, *Proc. R. Soc. A* **247**, 505 (1958).
- [5] W. C. Natzle and C. B. Moore, Recombination of H^+ and OH^- in pure liquid water, *J. Phys. Chem.* **89**, 2605 (1985).
- [6] B. L. Trout and M. Parrinello, The dissociation mechanism of H_2O in water studied by first-principles molecular dynamics, *Chem. Phys. Lett.* **288**, 343 (1998).
- [7] M. Sprik, Computation of the pK of liquid water using coordination constraints, *Chem. Phys.* **258**, 139 (2000).
- [8] P. L. Geissler, C. Dellago, D. Chandler, J. Hutter, and M. Parrinello, Autoionization in liquid water, *Science* **291**, 2121 (2001).
- [9] A. Hassanali, M. K. Prakash, H. Eshet, and M. Parrinello, On the recombination of hydronium and hydroxide ions in water, *Proc. Natl. Acad. Sci. U.S.A.* **108**, 20410 (2011).
- [10] M. Moqadam, A. Lervik, E. Riccardi, V. Venkatraman, B. K. Alsberg, and T. S. van Erp, Local initiation conditions for water autoionization, *Proc. Natl. Acad. Sci. U.S.A.* **115**, E4569 (2018).
- [11] C. Dellago, P. G. Bolhuis, F. S. Csajka, and D. Chandler, Transition path sampling and the calculation of rate constants, *J. Chem. Phys.* **108**, 1964 (1998).
- [12] J. D. Eaves, A. Tokmakoff, and P. L. Geissler, Electric field fluctuations drive vibrational dephasing in water, *J. Phys. Chem. A* **109**, 9424 (2005).
- [13] A. Laio and M. Parrinello, Escaping free-energy minima, *Proc. Natl. Acad. Sci. U.S.A.* **99**, 12562 (2002).
- [14] A. Barducci, G. Bussi, and M. Parrinello, Well-Tempered Metadynamics: A Smoothly Converging and Tunable Free-Energy Method, *Phys. Rev. Lett.* **100**, 020603 (2008).
- [15] J. Behler and M. Parrinello, Generalized Neural-Network Representation of High-Dimensional Potential-Energy Surfaces, *Phys. Rev. Lett.* **98**, 146401 (2007).
- [16] J. Behler, Atom-centered symmetry functions for constructing high-dimensional neural network potentials, *J. Chem. Phys.* **134**, 074106 (2011).

- [17] T. E. Markland and M. Ceriotti, Nuclear quantum effects enter the mainstream, *Nat. Rev. Chem.* **2**, 109 (2018).
- [18] See Supplemental Material at <http://link.aps.org/supplemental/10.1103/PhysRevLett.131.158001> for extended discussions on the methods and analysis, which included Refs. [5,9,19–53].
- [19] P. Tiwary and M. Parrinello, A time-independent free energy estimator for metadynamics, *J. Phys. Chem. B* **119**, 736 (2015).
- [20] V. Kapil *et al.*, i-PI 2.0: A universal force engine for advanced molecular simulations, *Comput. Phys. Commun.* **236**, 214 (2019).
- [21] O. Marsalek and T. E. Markland, Quantum dynamics and spectroscopy of *ab initio* liquid water: The interplay of nuclear and electronic quantum effects, *J. Phys. Chem. Lett.* **8**, 1545 (2017).
- [22] B. Reischl, J. Köfinger, and C. Dellago, The statistics of electric field fluctuations in liquid water, *Mol. Phys.* **107**, 495 (2009).
- [23] G. Kresse and J. Hafner, *Ab initio* molecular dynamics for liquid metals, *Phys. Rev. B* **47**, 558 (1993).
- [24] G. Kresse and J. Furthmüller, Efficient iterative schemes for *ab initio* total-energy calculations using a plane-wave basis set, *Phys. Rev. B* **54**, 11169 (1996).
- [25] P. E. Blöchl, Projector augmented-wave method, *Phys. Rev. B* **50**, 17953 (1994).
- [26] J. P. Perdew, J. A. Chevary, S. H. Vosko, K. A. Jackson, M. R. Pederson, D. J. Singh, and C. Fiolhais, Atoms, molecules, solids, and surfaces: Applications of the generalized gradient approximation for exchange and correlation, *Phys. Rev. B* **46**, 6671 (1992).
- [27] B. Hammer, L. B. Hansen, and J. K. Nørskov, Improved adsorption energetics within density-functional theory using revised Perdew-Burke-Ernzerhof functionals, *Phys. Rev. B* **59**, 7413 (1999).
- [28] S. Grimme, J. Antony, S. Ehrlich, and H. Krieg, A consistent and accurate *ab initio* parametrization of density functional dispersion correction (DFT-D) for the 94 elements H-Pu, *J. Chem. Phys.* **132**, 154104 (2010).
- [29] S. Sakong, K. Forster-Tonigold, and A. Groß, The structure of water at a Pt(111) electrode and the potential of zero charge studied from first principles, *J. Chem. Phys.* **144**, 194701 (2016).
- [30] T. Morawietz, A. Singraber, C. Dellago, and J. Behler, How van der Waals interactions determine the unique properties of water, *Proc. Natl. Acad. Sci. U.S.A.* **113**, 8368 (2016).
- [31] J.-P. Ryckaert, G. Ciccotti, and H. J. Berendsen, Numerical integration of the Cartesian equations of motion of a system with constraints: Molecular dynamics of n-alkanes, *J. Comput. Phys.* **23**, 327 (1977).
- [32] A. Singraber, Mpbircher, S. Reeve, D. W. Swenson, J. Lauret, and Philippedavid, *Compphysvienna/n2p2*: Version 2.1.4 (2021).
- [33] A. Singraber, J. Behler, and C. Dellago, Library-based LAMMPS implementation of high-dimensional neural network potentials, *J. Chem. Theory Comput.* **15**, 1827 (2019).
- [34] A. P. Thompson, H. M. Aktulga, R. Berger, D. S. Bolintineanu, W. M. Brown, P. S. Crozier, P. J. in 't Veld, A. Kohlmeyer, S. G. Moore, T. D. Nguyen, R. Shan, M. J. Stevens, J. Tranchida, C. Trott, and S. J. Plimpton, LAMMPS—a flexible simulation tool for particle-based materials modeling at the atomic, meso, and continuum scales, *Comput. Phys. Commun.* **271**, 108171 (2022).
- [35] L. B. Skinner, C. Huang, D. Schlessinger, L. G. M. Pettersson, A. Nilsson, and C. J. Benmore, Benchmark oxygen-oxygen pair-distribution function of ambient water from x-ray diffraction measurements with a wide Q-range, *J. Chem. Phys.* **138**, 074506 (2013).
- [36] I.-C. Yeh and G. Hummer, System-size dependence of diffusion coefficients and viscosities from molecular dynamics simulations with periodic boundary conditions, *J. Phys. Chem. B* **108**, 15873 (2004).
- [37] G. A. Tribello, M. Bonomi, D. Branduardi, C. Camilloni, and G. Bussi, PLUMED 2: New feathers for an old bird, *Comput. Phys. Commun.* **185**, 604 (2014).
- [38] E. Grifoni, G. Piccini, and M. Parrinello, Microscopic description of acid–base equilibrium, *Proc. Natl. Acad. Sci. U.S.A.* **116**, 4054 (2019).
- [39] E. Bitzek, P. Koskinen, F. Gähler, M. Moseler, and P. Gumbsch, Structural Relaxation Made Simple, *Phys. Rev. Lett.* **97**, 170201 (2006).
- [40] C. Zhang, F. Giberti, E. Sevgen, J. J. de Pablo, F. Gygi, and G. Galli, Dissociation of salts in water under pressure, *Nat. Commun.* **11**, 3037 (2020).
- [41] T. H. Cormen, C. E. Leiserson, R. L. Rivest, and C. Stein, *Introduction to Algorithms*, 4th ed. (MIT Press, Cambridge, MA, 2022).
- [42] M. Ceriotti and D. E. Manolopoulos, Efficient First-Principles Calculation of the Quantum Kinetic Energy and Momentum Distribution of Nuclei, *Phys. Rev. Lett.* **109**, 100604 (2012).
- [43] A. Luzar and D. Chandler, Effect of Environment on Hydrogen Bond Dynamics in Liquid Water, *Phys. Rev. Lett.* **76**, 928 (1996).
- [44] X. Yang, Y. Wu, S. Deng, Y. Gao, L. Liu, and C. Liu, Characterizing the transient structures of hydrated proton in solution by machine-learning enhanced power spectrum assignment method (to be published).
- [45] D. Muñoz-Santiburcio, Accurate diffusion coefficients of the excess proton and hydroxide in water via extensive *ab initio* simulations with different schemes, *J. Chem. Phys.* **157**, 024504 (2022).
- [46] T. S. Light, S. Licht, A. C. Bevilacqua, and K. R. Morash, The fundamental conductivity and resistivity of water, *Electrochem. Solid-State Lett.* **8**, E16 (2004).
- [47] S. H. Lee and J. C. Rasaiah, Proton transfer and the mobilities of the H^+ and OH^- ions from studies of a dissociating model for water, *J. Chem. Phys.* **135**, 124505 (2011).
- [48] A. J. Cohen, P. Mori-Sánchez, and W. Yang, Insights into current limitations of density functional theory, *Science* **321**, 792 (2008).
- [49] J. N. Brønsted, Einige bemerkungen über den begriff der säuren und basen [some observations about the concept of acids and bases], *Recl. Trav. Chim. Pays-Bas* **42**, 718 (1923).
- [50] T. M. Lowry, The uniqueness of hydrogen, *J. Soc. Chem. Ind.* **42**, 43 (1923).
- [51] P. P. Ewald, Die berechnung optischer und elektrostatischer gitterpotentiale, *Ann. Phys. (N.Y.)* **369**, 253 (1921).

- [52] A. Y. Toukmaji and J. A. Board, Ewald summation techniques in perspective: A survey, *Comput. Phys. Commun.* **95**, 73 (1996).
- [53] P. Bultinck, C. Van Alsenoy, P. W. Ayers, and R. Carbó-Dorca, Critical analysis and extension of the Hirshfeld atoms in molecules, *J. Chem. Phys.* **126**, 144111 (2007).
- [54] D. Sheppard, R. Terrell, and G. Henkelman, Optimization methods for finding minimum energy paths, *J. Chem. Phys.* **128**, 134106 (2008).
- [55] D. G. Truhlar, W. L. Hase, and J. T. Hynes, Current status of transition-state theory, *J. Phys. Chem.* **87**, 2664 (1983).
- [56] J. L. Bao and D. G. Truhlar, Variational transition state theory: Theoretical framework and recent developments, *Chem. Soc. Rev.* **46**, 7548 (2017).
- [57] T. Joutsuka, Molecular mechanism of autodissociation in liquid water: *Ab initio* molecular dynamics simulations, *J. Phys. Chem. B* **126**, 4565 (2022).
- [58] M. J. S. Dewar, Multibond reactions cannot normally be synchronous, *J. Am. Chem. Soc.* **106**, 209 (1984).
- [59] A. D. McNaught and A. Wilkinson, synchronous, in *The IUPAC Compendium of Chemical Terminology* (Blackwell Scientific Publications, Oxford, 1997).
- [60] Z. Yang, C. S. Jamieson, X.-S. Xue, M. Garcia-Borràs, T. Benton, X. Dong, F. Liu, and K. Houk, Mechanisms and dynamics of reactions involving entropic intermediates, *Trends Chem.* **1**, 22 (2019).
- [61] D. Marx, M. E. Tuckerman, J. Hutter, and M. Parrinello, The nature of the hydrated excess proton in water, *Nature (London)* **397**, 601 (1999).
- [62] M. E. Tuckerman, D. Marx, and M. Parrinello, The nature and transport mechanism of hydrated hydroxide ions in aqueous solution, *Nature (London)* **417**, 925 (2002).
- [63] T. C. Berkelbach, H.-S. Lee, and M. E. Tuckerman, Concerted Hydrogen-Bond Dynamics in the Transport Mechanism of the Hydrated Proton: A First-Principles Molecular Dynamics Study, *Phys. Rev. Lett.* **103**, 238302 (2009).
- [64] H. J. C. Berendsen, J. R. Grigera, and T. P. Straatsma, The missing term in effective pair potentials, *J. Phys. Chem.* **91**, 6269 (1987).